Laser Dazzling of Focal Plane Array Cameras

Ric (H.)M.A. Schleijpen[1], Johan C. van den Heuvel[1], Arjan L. Mieremet[1],
Benoit Mellier[2], Frank J.M. van Putten[1]
[1]TNO Defence, Security and Safety, P.O. Box 96864, 2509 JG The Hague, The Netherlands
[2]CELAR, Division DIRAC, 35170 Bruz, France,

ABSTRACT

Laser countermeasures against infrared focal plane array cameras aim to saturate the full camera image. In this paper we will discuss the results of three different dazzling experiments performed with MWIR lasers and show that the obtained results are independent of the read-out mechanism of the camera and can be explained by an expression derived from the point spread function of the optics. This expression also allows us to estimate the required laser power to saturate a complete focal plane array in a camera system. Simulated Images with simulated dazzling effects based on this expression will be shown.

Keywords: Laser dazzling, Focal plane array cameras, Countermeasures, Infrared.

1. INTRODUCTION

Recent developments in laser technology have made MWIR lasers available for the use in Directed Infrared Countermeasure (DIRCM) systems. DIRCM systems are mounted on board of aircraft for platform self protection and are mainly designed for use against current anti-aircraft missiles, based on reticule or scanning seeker technology. In this way infrared seekers can be deceived. However, the next generation infrared missiles will use imaging seekers. In general deceiving is no then no longer possible and dazzling with a continuous laser source is in that case considered as a potential countermeasure. Dazzling causes a reversible saturation effect on the detector array. At ranges between a few hundred to a few thousand meters, most of the current MWIR lasers provide irradiance levels, which do not exceed dazzling effects. For permanent damage much higher irradiance levels are needed. In this paper we will not address damage effects but focus on dazzling effects.

The countermeasure application of MWIR lasers is not limited to missile seekers. In this paper we therefore will discuss the dazzle effects of DIRCM like laser systems on imaging systems in general. The paper is organized as follows; in section 2 we start with a description of three different experimental set-ups that have been used for dazzling experiments. In section 3 we will discuss the results for the three camera systems with different detector materials. Section 4 will present theoretical considerations which show that the observed dazzling effects can be attributed to optical mechanisms. This section will also provide methods to estimate the size of the saturated area in the image. In section 5 we will show some images with simulated dazzling effects following the theory in section 4 and we finish with our main conclusions in section 6.

2. EXPERIMENTAL SET-UP

Dazzling experiments were performed with different combinations of infrared focal plane array cameras and different MWIR lasers. The three combinations that are described below use different types of detectors, namely a CMT camera, an InSb camera and a PtSI camera. Each of the three set-ups was used at a different location, which allowed us to vary the range between camera and laser from less than 1 meter up to 275 meters.

ric.schleijpen@tno.nl phone +31 70 374 0045, fax +31 70 374 0654, www.tno.nl

Infrared Imaging Systems: Design, Analysis, Modeling, and Testing XVIII,
edited by Gerald C. Holst, Proc. of SPIE Vol. 6543, 65431B, (2007)
0277-786X/07/$18 · doi: 10.1117/12.718602

2.1. CMT camera and DF laser

The CMT camera is an infrared imaging seeker simulator system as described in reference 1. This system is basically an infrared camera with a unit for steering the field of view. The field of view of the camera is 4.4° x 4.4° covered by a 256 x 256 detector array with snap-shot read-out. The field of view is steered by a Risley prism unit (reference 2). This field-of-view steering unit adds extra optical elements to the system, which may cause scatter effects in the optics to appear stronger than in usual camera optics. Apart from the extra lenses the Risley prisms alone add eight optical elements.

The laser is a CW DF chemical laser modulated by an acousto-optic cell. This laser setup combined with calibrated attenuators enabled to generate controlled levels of CW laser output or controlled laser pulse sequences like in a jammer. For a more complete description of the experimental set-up see reference 1. During the experiments, the laser was operated both in CW mode and pulse mode, the latter with various pulse frequencies (5 and 20 kHz) and various pulse durations between 5 μs and 100 μs.

During all laser tests, the camera had a fixed 1 ms integration time and 100 Hz frame rate for the detector array. The laser irradiance levels on the seeker varied from 10^4 pW/cm^2 to 10^7 pW/cm^2. This range covers typical DIRCM laser irradiance levels on seekers, taking into account typical values for the laser power, the laser beam divergence and the engagement range. The upper level was selected to avoid damage to the detector. For all the tests the laser was aligned along the seeker boresight in order to avoid ghost images which could disturb the interpretation of the test results.

2.2. InSb camera and PPNL OPO laser

The InSb camera is a standard 256 x 320 array camera with narrow (1.5° x 2.0°) and wide (4.5° x 6.0°) field of view optics. The camera is used at a fixed integration time and standard NTSC frame rate. The laser is a PPLN OPO laser pumped by a Nd:YVO_4 laser as described in reference 3. The laser pulse length is typically in the 1-100 ns regime, while the pulse repetition frequency is determined by the PRF of the pump laser which is set to 30 kHz. This pulse rate ensures that there are a significant number of pulses within the camera integration time of typically 1 msec. It is interesting to note that the minimum laser pulse duration generated with the PPNL OPO laser is about two orders of magnitude less than those of the DF laser. Calibrated attenuators enable us to control the laser irradiance levels on the camera over more than 4 orders of magnitude. The maximum un-attenuated laser power caused some semi-permanent effects which disappeared after a thermal cycle to room temperature for the detector assembly. The experiments were performed in an indoor test range of 300 m length. The maximum distance between the laser and the camera in the experiments was 275 m. Again the laser was aligned along the seeker boresight in order to avoid ghost images.

Some additional experiments were performed with a scanning InSb camera. In this camera a staggered linear detector array scans the field of view in this system. This camera was used to compare the saturation effects on a camera system with a completely different electronic read-out mechanism.

2.3. PtSi camera and PPNL OPO laser

The PtSi camera for the experiments is a standard camera with 16° x 16° field of view with a 256 x 256 array. The camera used a fixed integration time and 30 Hz frame rate. The same PPLN OPO laser is used as for the InSb camera experiments. The distance between the laser and the camera in the experiments was approximately 1 m. The camera focus was adjusted to compensate for residual laser beam divergence. Due to the low quantum efficiency of PtSi also the maximum un-attenuated laser power could be irradiated on the camera without causing permanent damage to the camera.

3. RESULTS DAZZLE EXPERIMENTS

3.1. CMT camera with DF laser

The impact of the laser irradiance on the CMT camera images is illustrated in figure 1. For the “on-axis” irradiance there are no “ghost” images even for the highest levels of laser irradiance. The spot next to the laser spot which is visible in the images for the lowest irradiance levels is a black body source used for pointing the seeker simulator. The dazzling spot is nearly circular. The diameter of the dazzled area is 8 pixels for a laser irradiance of 10^5 pW/cm^2 at the front optics of the camera. The size of the dazzled area increased up to a diameter of about 60 pixels for a laser irradiance of 10^7 pW/cm^2. The diameter is measured at half the saturation level. At the higher irradiance levels a grey shadow and radial spikes

become visible outside the saturated area. A large variety of laser pulses that have been tested, the size of the observed laser spot diameter as a function of laser irradiance averaged over the pulses is plotted in figure 2.

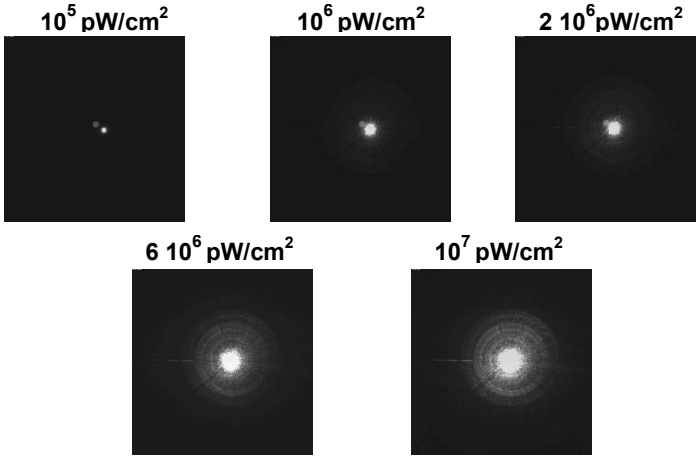

Figure 1: Impact of various DF laser irradiance levels on the CMT camera image (CW power)

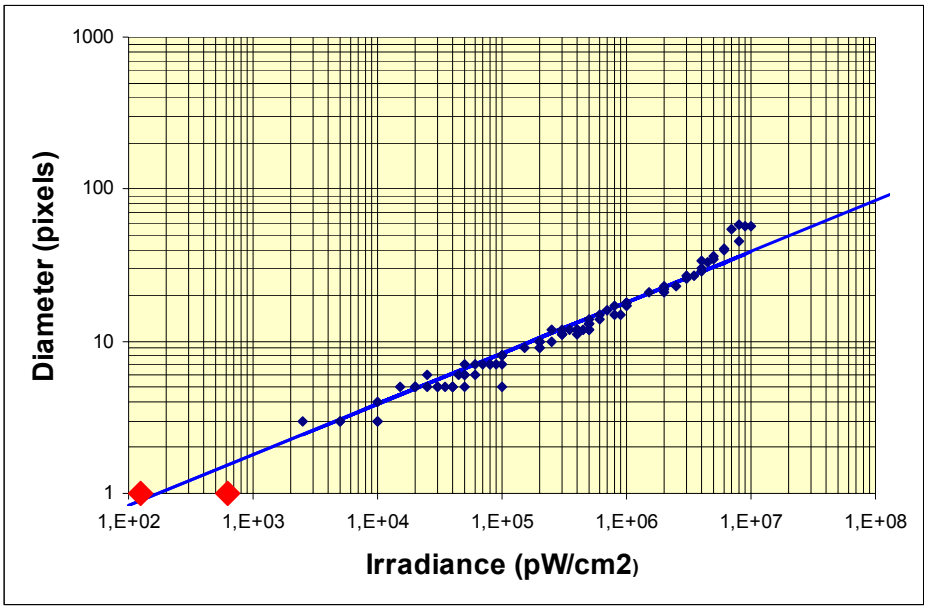

Figure 2: Observed laser dazzle area diameter in the CMT camera image as a function of DF laser irradiance.

The graph of figure 2 shows two interesting features; a) the solid line through the data (small diamonds) has a slope of 1/3 and b) for the high irradiance levels the diameter of the dazzling area starts to grow faster than indicated by the solid line. For these high irradiance levels a line with a slope of roughly 1/2 would be more appropriate.

The slope of 1/3 indicates the following empirical rule: increasing the power by a factor 8 will increase the saturated spot size by a factor 2. This rule seems to cover almost the full range of the experimental results except for the very high irradiance levels. The maximum saturated spot size obtained in the experiments is 60 pixels in diameter. According to the experimental rule one would need 64 times more laser power to saturate the whole detector of 256 x 256 pixels. An irradiance level of 64 10^7 pW/cm^2 would yield a spot diameter of 4 x 60 pixels. Unfortunately these levels were not tested because they were above the estimated range for safe operation of the laser without risk for damage to the detector. We decided to keep at least one order of magnitude of margin to the range of potential detector damage.

The large diamonds in figure 2 mark the estimates for the irradiance level where a single pixel is just saturated. The two markers were derived following two different calculation methods. The first approach uses the following data on the camera: F# 2.8, focal length f = 100 mm, transmission of the optics $\tau_{optics} = 0.5$, fill factor 0.9, quantum efficiency $\eta = 0.65$, detector well capacity $3.7\ 10^7$ electrons. For the given F# and focal length of the optics the entrance pupil area is than 10 cm^2. We assume that all the laser energy from the point source hits only one detector and all the incoming photons are transferred to the capacitor after conversion. This approximation assumes a narrow point spread function which is justified for this rough estimation. Given the well capacity of $3.7\ 10^7$ electrons, $3.7\ 10^7$ / (0.65 x 0.9 x 0.5) photons need to enter the optics for saturation. For the 10 cm^2 entrance pupil this is $1.26\ 10^7$ photons/ cm^2. This is the number of photons during 1 msec integration time. At 4 μm we have 5×10^{-20} J/photon. For the saturation irradiance level we then obtain 5×10^{-20} J/photon x $1.26\ 10^{10}$ photons / sec / cm^2 = 625 pW/cm^2.

The second approach derives the saturation level from the scene temperature where the array saturates. In a separate experiment this temperature was measured to be at 385 K. In the 3.7 - 4.8 μm pass band the detector then "sees" 13.78 W/m^2/sr black-body radiance. A square 0.3 mrad IFOV (Instantaneous Field Of View) area as "seen" by a single detector then delivers an irradiance of 124 pW/cm^2 on the camera lens. As can be seen in figure 2, both estimates for the saturation levels are close to the extrapolation of the experimental saturation data using the empirical rule.

3.2. InSb camera with a PPLN OPO laser

In figure 3 we show some images of the InSb camera irradiated by the PPLN OPO laser for different irradiance levels. The images shown are collected for the camera set in the narrow field of view mode and with the laser positioned in the centre of the field of view. Additional data were collected for the wide field of view mode and for 1° and 3° off-centre laser positions. These angles correspond to laser positions at the edge of the narrow and wide field of view, respectively.

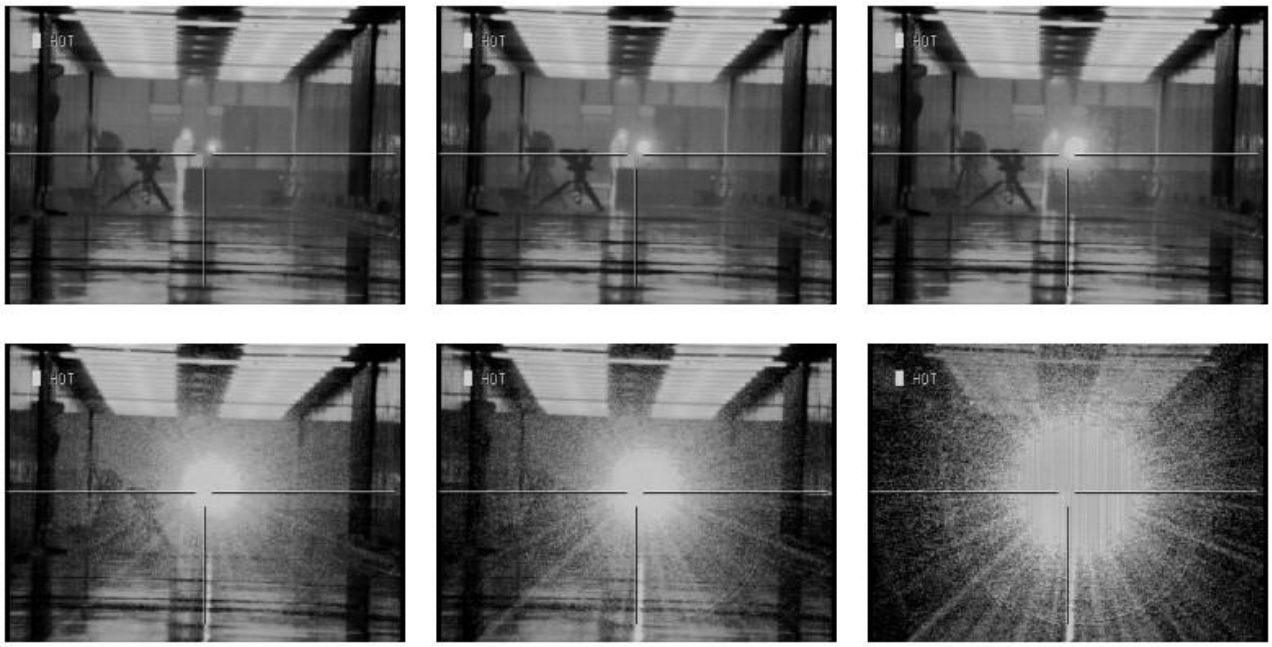

Figure 3: Impact of various laser irradiance levels on the narrow field of view InSb camera image. Laser attenuation levels in neutral density: 4.4, 3.3, 2.6 top left to right, 1.3, 0.6, 0.0 bottom left to right.

In figure 4 we have plotted the diameter of the saturated area versus the irradiance for this camera. The upper two curves (blue) are for the narrow field of view, while the lower set of curves (red) is for the wide field of view. A "dip" is clearly visible in all curves at $2.5\ 10^2$. This caused by bad alignment of the 0.6 neutral density filter, which causes a deflection of the laser beam. Since we used combinations of ND filters, the same "dip" occurs at other intensity levels, but less prominent. The solid curves are best fits to the data and have a slope of 0.32. This implies that the size of the saturated area increases with the irradiance to the power 0.32. This is once more in agreement with the empirical rule found in figure 2.

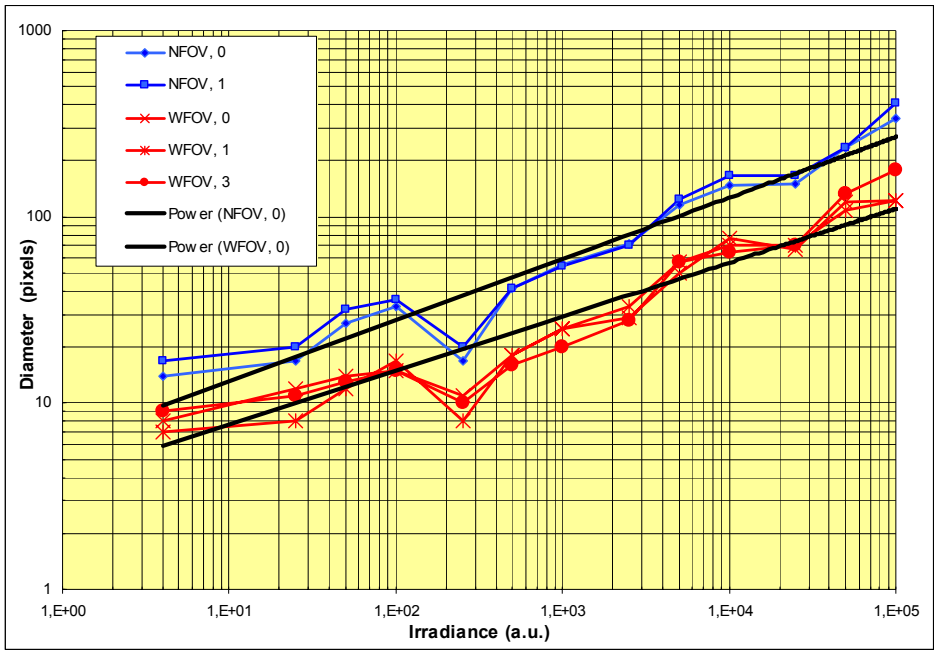

Figure 4: Observed laser dazzle area diameter in the InSb camera as a function of laser irradiance for narrow field of view (blue - top) and wide field of view (bottom – red).

3.3. PtSi camera with a PPLN OPO laser

Figure 5 shows some samples of the PPLN OPO laser dazzling effects on the PtSi camera. Apart from the saturated centre area two other effects can be observed. In the left part of figure 5 a cross like scatter pattern is observed with the saturated area in the centre. This typical cross pattern is observed in other PtSi cameras from other manufacturers as well. These effects are attributed to optical effects because the straight lines do not follow the vertical of horizontal geometry of the detector read-out circuit as high intensity effects in visible cameras do. Still the effects may be related to the read-out circuit, because only for PtSi cameras the detector is on the same chip as the read-out circuit and not separated as for the CMT and InSb camera. The periodic structures in the readout structure might therefore cause such patterns. The right hand part of figure 5 also shows ring like structures. These structures are observed only for the highest irradiance levels. We believe these are related to the scatter in the diffractive optics of the camera.

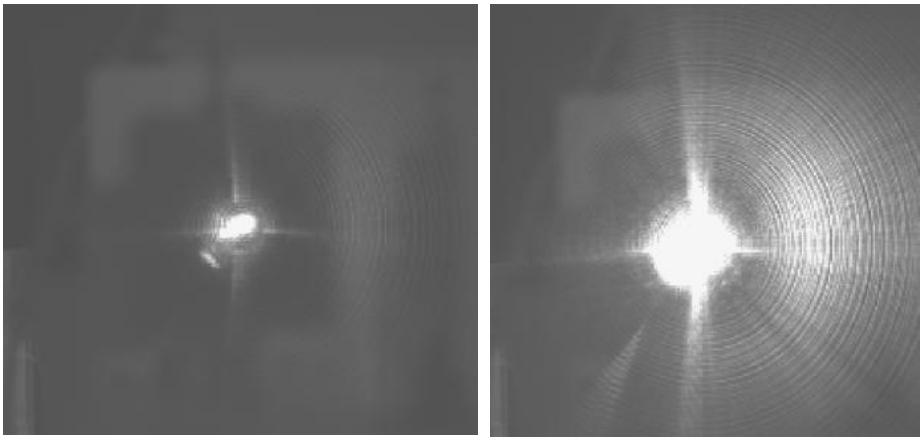

Figure 5: Samples of the impact of laser irradiance on the PtSi camera.

Figure 6 plots the diameter of the saturated area versus the irradiance for this camera. The different data point symbols represent the values measured for the vertical and horizontal diameter of the saturated area. The straight line has a slope of 1/3 and result form using the same empirical rule as in figure 2. Strong deviations are already observed at relatively low irradiance levels compared to the CMT and InSb camera. These deviations are attributed to the scatter effects in this camera as discussed above.

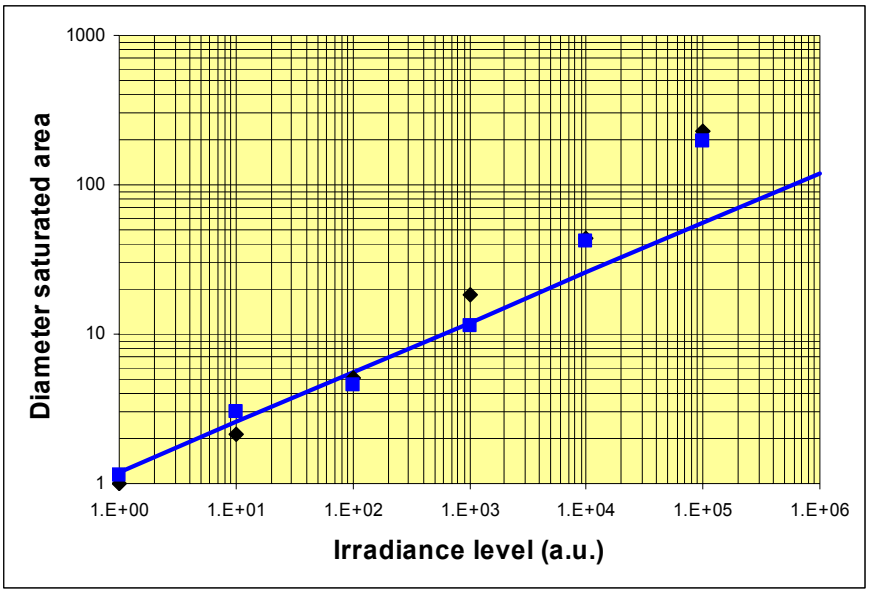

Figure 6: Observed laser dazzle area diameter in the PtSi camera as a function of laser irradiance.

4. AREA OF SATURATION

The examples above show that the infrared cameras continue to operate over a large dynamic range of irradiance levels without problems in the readout circuit. In similar studies for visible light cameras the read out circuit often shows failures at lower intensities, long before the full image is saturated. Moreover, the example of the scanning InSb camera indicates that the saturation effects are independent of the read-out mechanism. Therefore, the potential effects in the read-out circuit are not discussed here. Instead, we will derive an expression for the radius of the saturated area (x_{sat}) in an image as a function of the power of the laser (I_0) based on optical effects only. This derivation nicely explains the empirical rule and can also explain the increasing growth of the saturated area for high irradiance levels.

4.1. Diffraction limited point spread function

The image of a point source is well described by the point spread function (PSF). For diffraction limited circular optics, the PSF is given by the Airy function:

$$PSF(x) = \left(\frac{2J_1(x)}{x} \right)^2, \tag{1}$$

where x is some radial coordinate depending on wavelength and the numerical aperture of the optic and J_1 is the first order Bessel function of the first kind. For low intensity sources we are usually only interested in the PSF values for small distances x from the centre of the point source in the focal plane. However, in the case of dazzling, we are also interested in the behavior of the PSF far from the central peak. Far from the central peak, i.e. when $x >> 1$, the Bessel function J_1 can be approximated by (reference 4):

$$J_1(x) \approx \sqrt{\frac{2}{\pi x}} \cos\left(x - \frac{3\pi}{4} \right). \tag{2}$$

Substitution of this expression into Eq.(1) yields:

$$PSF(x) \approx \frac{8}{\pi x^3}\cos^2\left(x - \frac{3\pi}{4}\right), \tag{3}$$

where the $\cos^2$-term describes the oscillating behavior of the Airy function, while the pre-factor determines the peak intensity of the rings. In a typical camera system the distances between the dark rings are comparable in size to the pixel dimensions. This implies that the camera will not resolve the dark rings and the average of $\cos^2$ can be taken, which is 1/2. The PSF can then be described by:

$$PSF(x) \approx \frac{4}{\pi x^3}. \tag{4}$$

A plot of the original Airy function, Eq. (1), and this approximation are shown in the top left panel of figure 7. Note that for small x the approximation no longer holds. As it is known that the PSF converges to 1 for small values of x, we propose the following approximation instead:

$$PSF(x) \approx \frac{4}{\pi x^3 + 4}. \tag{5}$$

This approximation is shown in the center left panel of figure 7. When the threshold for saturation is given by I_{sat}, we can derive the relation between size of the saturated area in the image and irradiance, by putting $I_{sat} = I_0\, PSF(x_{sat})$, where I_0 is the irradiance of the laser in the center of the PSF. Rewriting this equation gives us the following expression for the size of the saturated area:

$$x_{sat} = \sqrt[3]{\frac{4}{\pi}\left(\frac{I_0}{I_{sat}} - 1\right)}. \tag{6}$$

A plot of this function is shown in the center right panel of figure 7. Comparing this with the top right panel shows that for $I_0/I_{sat} < 1$ no area is saturated, which is as expected. In practice it will be impossible to observe this part of the curve since it is the area of saturation has no meaning on a sub-pixel level. Also the typical errors in the measurements do not allow these types of precision measurements. This means that we can only observe the part of the curve where $x_{sat} > 1$.

The most important conclusion that can be drawn from this expression is the fact that x_{sat} is proportional with $I_0^{1/3}$, which confirms the empirical rule found from the measurements. This expression however does not explain the increased growth for large irradiance levels.

4.2. Scatter

For high irradiance levels the size of the saturated area deviates from the values predicted by the expression derived in the previous section. Often a more rapid increase is observed. This comes from the fact that scattering in the optic becomes important. In this section we derive an expression for x_{sat} including a scatter term.

We assume that the entrance lens of the camera scatters a fraction ρ of the incident radiation. The scattered radiation from one point on the entrance lens is normally distributed around the original point in the image plane. The distribution of all scattered radiation in the image plane can then be calculated by taking the convolution of the scatter distribution with the pupil function. The exact shape of the scatter distribution as a function of x depends on many factors. Scatter in other optical elements and multiple reflections add even more complexity. For illustration we use a simple approach: we assume that the scatter distribution is at a (low) constant level ρ over the focal plane. Including this "scatter floor in the PSF the function then becomes:

$$PSF(x) \approx (1-\rho)\frac{4}{\pi x^3 + 4} + \rho, \tag{7}$$

where the first term is caused by diffraction and the second term by scatter. For small values of ρ, it is reasonable to assume that the (1-ρ) prefactor can be neglected. When doing so, one can show that:

$$x_{\text{sat}} = \sqrt[3]{\frac{4}{\pi}\left(\frac{I_0}{I_{\text{sat}} - \rho I_0} - 1\right)} \quad (8)$$

To see the effects of the additional scatter-term we have plotted Eq.(7) in the bottom left panel and Eq.(8) in the bottom right panel of figure 7 assuming $\rho = 0.0015$. Once more we see that $x_{\text{sat}} \propto I_0^{1/3}$ when $\rho I_0 << I_{\text{sat}}$, however at high irradiance levels a fast growth in x_{sat} is expected since $I_{\text{sat}} - \rho I_0$ goes to zero. In general, if we had taken the scatter distribution of the form ρx^{-n}, with n some positive real value, x_{sat} would be of the form $(I_0/I_{\text{sat}})^{1/n}$ for $\rho I_0 \sim I_{\text{sat}}$. For high irradiance levels the slope of $x_{\text{sat}}(I_0/I_{\text{sat}})$ thus depends on the scatter distribution of the optics.

It should be noted that the scatter as described by Eq. (7) shows a monotonous decrease in intensity down to a constant intensity when moving from the centre of the laser spot towards the edges of the field of view. It is obvious that the distribution within the saturated area cannot be checked, be the size of the saturated area does seem to support this description. Inspection of the non-saturated part of the image shows that the intensity level is not evenly distributed. However, the average level could be well described by Eq. (7).

In this section we have derived an expression for the size of the saturated area in an image of a camera that is irradiated by a laser, which explains the measurements shown in the previous section. Note that no assumptions have been made about the read-out mechanism and detector material to derive this expression, indicating that the area of saturation is also independent of these parameters and mostly determined by optical mechanisms.

5. SIMULATED SATURATION

As an illustration we simulated the effect of laser dazzling. As the starting point we use the undisturbed image in the upper left corner of figure 3. Keeping the dynamic range of the image unchanged, we add the laser intensity distribution over the focal plane array as described by Eq. (4). The results are shown in figure 8. The simulated laser irradiance at the camera aperture was increased in the same steps as the increase in figure 3. The results show great similarity to the effects in figure 3 except for the scatter behavior. Using the theoretical approach above, the intensity of the scatter in the image can only be described in the average values. As has been observed in the experiments the actual scatter is much more complex. This complexity of the scatter mechanisms cannot yet be simulated by our model and therefore we did not include this in the simulations.

6. CONCLUSION

In this paper we have shown experimental results of laser dazzling effects in infrared focal plane array cameras with three different detector materials. It has been shown for these cameras that the increase of the saturated area with increasing laser irradiance is independent of the read-out circuit over a large dynamic range.

An equation based on the optical point spread function is derived for the size of the saturated area as a function of the laser irradiance at the front optics. The experimental results tend to be well explained by this equation. This equation allows making estimations for the laser power levels needed to saturate a complete focal plane array in a camera system. This will support the work on the evaluation of laser dazzling effectiveness.

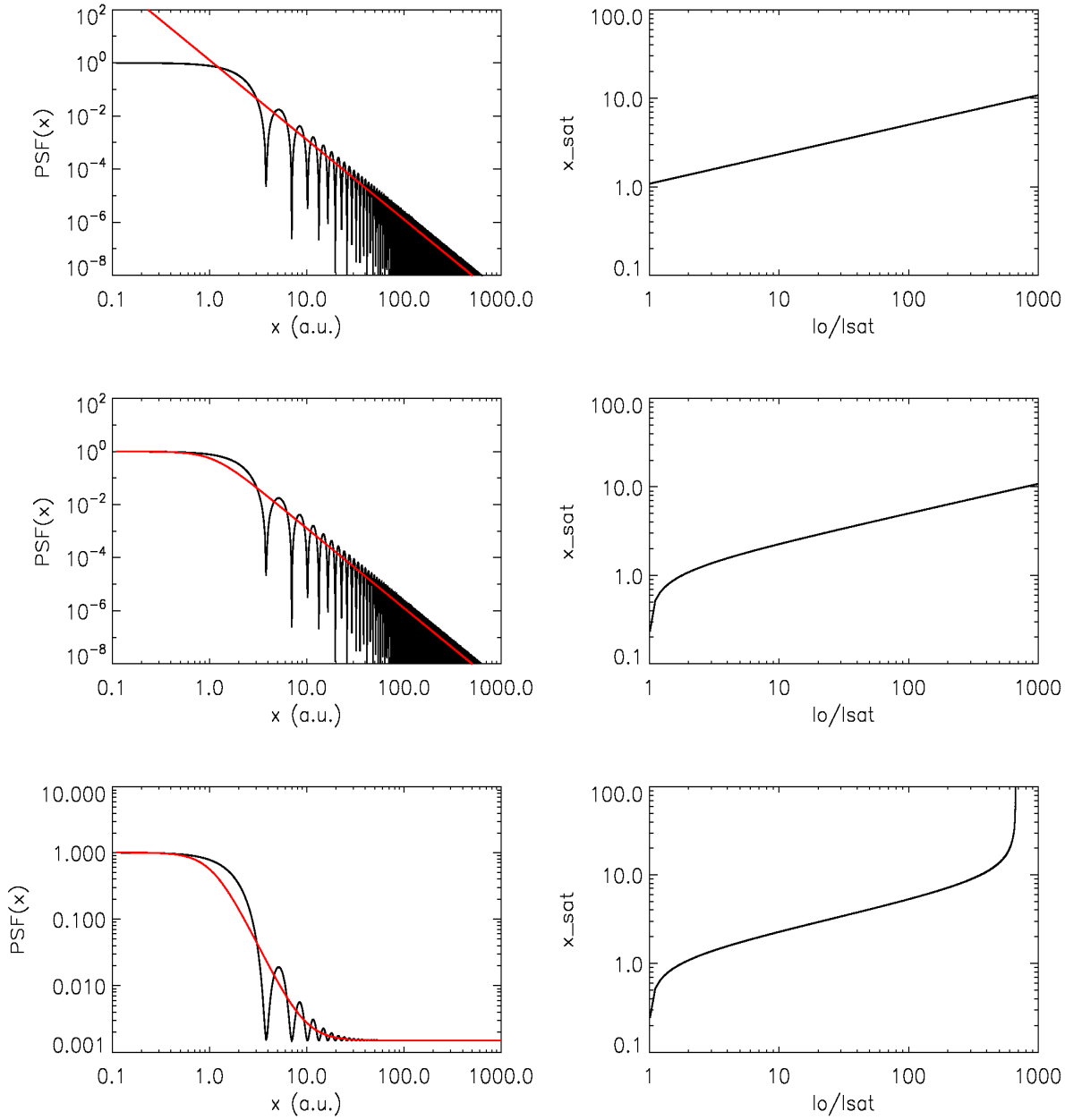

Figure 7: The left panels show the Airy function (black) and its approximation (red). The right panels show the corresponding size of the saturated area as a function of the ratio between the irradiance level and saturation irradiance.

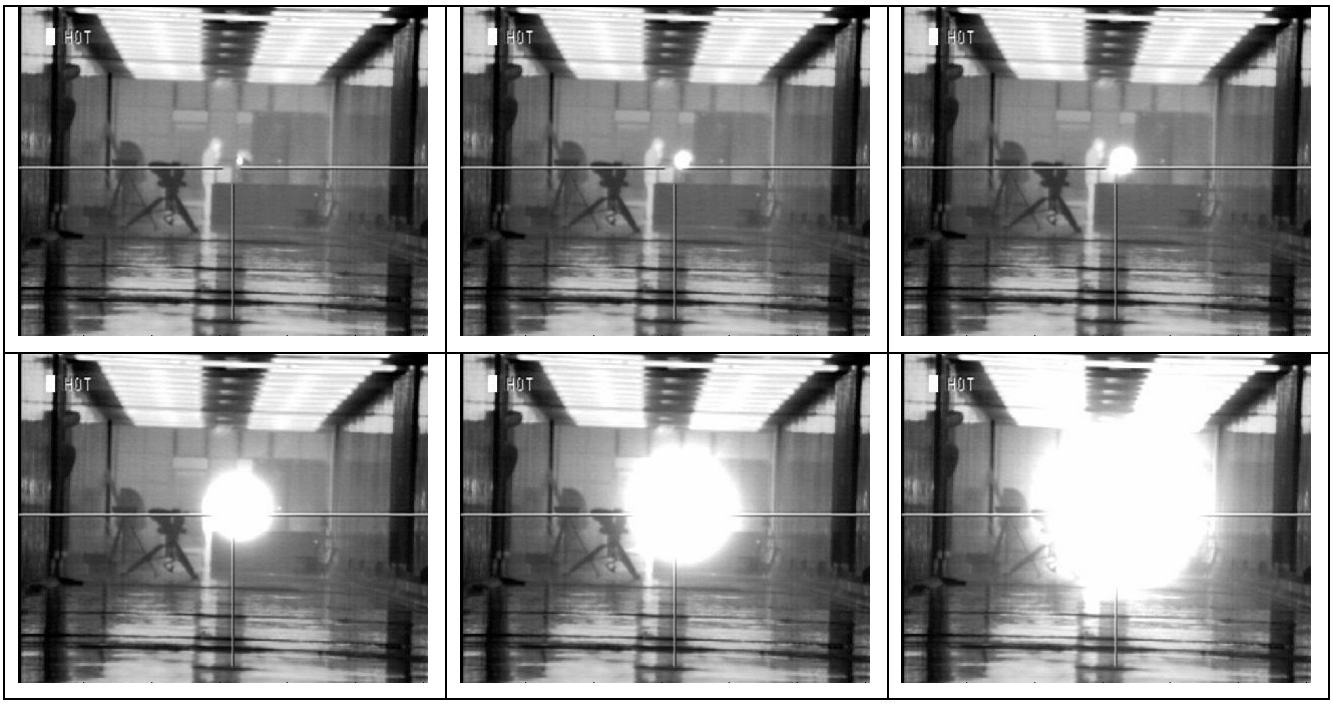

Figure 8 Simulated impact of various laser irradiance levels on the narrow field of view InSb camera image. Laser attenuation levels in neutral density 4.4, 3.3, 2.6 top left to right, 1.3, 0.6, 0.0 bottom left to right.

7. ACKNOWLEDGEMENT

This work was performed as a part of the Electronic Warfare programme V408 at TNO for the Royal Netherlands Air Force sponsored by the Netherlands MoD. The Royal Netherlands Army is acknowledged for providing camera systems for experiments. Helpful comments on scatter by Dr. L.J. Cox from Dstl, Sensors & Countermeasures Department, Farnborough, UK are gratefully acknowledged.

REFERENCES

1. H.M.A. Schleijpen, S.R. Carpenter, B. Mellier, A. Dimmeler: “Imaging Seeker Surrogate for IRCM evaluation”, SPIE Vol 6397: Technologies for Optical Countermeasures III, Stockholm, September 2006.
2. B.D. Duncan, “Wide-angle achromatic prism beam steering for infrared countermeasure applications”, Opt. Eng. 42(4), 1038-1047 April 2003.
3. H.H.P.Th. Bekman, J.C. van den Heuvel, F.J.M van Putten, H.M.A. Schleijpen, “Development of a Mid-Infrared Laser for Directed Infrared Countermeasures”’ London, Technologies for Optical Countermeasures, SPIE Vol 5614-03.
4. M.Abramowitz and I.A.Stegun, Handbook of Mathematical Functions, Us dept of Commerce, National Bureau of Standards, 1964.